International Journal of Geo-Information

MDPI

Article

Multiscale Visualization of Surface Motion Point Measurements Associated with Persistent Scatterer Interferometry

Panagiotis Kalaitzis [1], Michael Foumelis [2], Antonios Mouratidis [2,3], Dimitris Kavroudakis [1] and Nikolaos Soulakellis [1,*]

[1] Department of Geography, University of the Aegean, 81100 Mytilene, Greece; p.kalaitzis@geo.aegean.gr (P.K.); dimitrisk@aegean.gr (D.K.)
[2] Department of Physical and Environmental Geography, Aristotle University of Thessaloniki, 54124 Thessaloniki, Greece; mfoumelis@geo.auth.gr (M.F.); amourati@geo.auth.gr (A.M.)
[3] Center for Interdisciplinary Research and Innovation-Aristotle University of Thessaloniki (CIRI-AUTh), 57001 Thermi, Greece
* Correspondence: nsoul@aegean.gr

Abstract: Persistent scatterer interferometry (PSI) has been proven to be a robust method for studying complex and dynamic phenomena such as ground displacement over time. Proper visualization of PSI measurements is both crucial and challenging from a cartographic standpoint. This study focuses on the development of an interactive cartographic web map application, providing suitable visualization of PSI data, and exploring their geographic, cartographic, spatial, and temporal attributes. To this end, PSI datasets, generalized at different resolutions, are visualized in eight predefined cartographic scales. A multiscale generalization algorithm is proposed. The automation of this procedure, spurred by the development of a web application, offers users the flexibility to properly visualize PSI datasets according to the specific cartographic scale. Additionally, the web map application provides a toolset, offering state-of-the-art cartographic approaches for exploring PSI datasets. This toolset consists of exploration, measurement, filtering (based on the point's spatial attributes), and exporting tools customized for PSI measurement. Furthermore, a graph tool, offering users the capability to interactively plot PSI time-series and investigate the evolution of ground deformation over time, has been developed and integrated into the web interface. This study reflects the need for appropriate visualization of PSI datasets at different cartographic scales. It is shown that each original PSI dataset possesses a suitable cartographic scale at which it should be visualized. Innovative cartographic approaches, such as web applications, can prove to be effective tools for users working in the domain of mapping and monitoring the dynamic behavior of surface motion.

Keywords: web mapping applications; cartography; persistent scatterer interferometry (PSI); ground deformation; cartographic generalization

Citation: Kalaitzis, P.; Foumelis, M.; Mouratidis, A.; Kavroudakis, D.; Soulakellis, N. Multiscale Visualization of Surface Motion Point Measurements Associated with Persistent Scatterer Interferometry. *ISPRS Int. J. Geo-Inf.* **2024**, *13*, 236. https://doi.org/10.3390/ijgi13070236

Academic Editors: Wolfgang Kainz and Florian Hruby

Received: 14 February 2024
Revised: 12 June 2024
Accepted: 26 June 2024
Published: 2 July 2024

1. Introduction

Due to the rapid increase in the availability of earth observation (EO) data, a challenging demand emerges for precise, user-friendly, and interactive cartographic tools to facilitate the thorough exploration of these (big) EO data. In many cases, the interpretation of such information still remains a challenging process [1]. On the other hand, cartographic tools offer precise, swift, and low-cost approaches for analyzing and interpreting geospatial data. Additionally, the field of geospatial data visualization has made significant progress in recent years [2].

When delving into ground deformation and instability phenomena, the need for systematic detection, monitoring, and visualization arises. PSI is one of the most useful techniques for studying dynamic phenomena, and it is utilized throughout different fields, including geosciences, urban planning, and environmental disciplines, improving the comprehension of the earth's dynamic processes and strengthening the ability to reduce

associated hazards [3,4]. This method is based on spaceborne synthetic-aperture radar (SAR) imagery, offering precise monitoring of ground deformation over time. PSI provides important insights into a wide range of phenomena, such as land subsidence, landslides, volcanic activity, mining, and infrastructure stability [5]. The PSI method offers millimeter accuracy ground deformation measurements, with wide spatial coverage, at low-cost, and independent of ground-based installations [6]. It is a method offering sensitivity, even to subtle ground displacements, that has been well established through a plethora of studies (e.g., [4,7–16]) as one of the most frequently utilized approaches for accurate earth observation (EO)-based ground deformation measurements.

Persistent scatterers (PSs) are typically man-made structures or natural features with consistent radar reflectivity over time. Although they allow for robust measurements, they are limited in spatial density, as they are relatively sparse in non-urban environments and are dependent upon the availability of suitable targets within the radar scene. The inherent challenge of identifying PS targets restricts the applicability of the PSI technique in rapidly changing environments. The exploitation of the statistical properties of the radar signal from numerous randomly distributed targets within the radar resolution cell exhibiting "similar" scattering mechanism led to the development of the distributed scatterers (DS) approaches [17–19]. DS targets offer a significantly denser spatial coverage compared to PS, making it particularly advantageous in areas with sparse point-like scatterers and denser vegetation. DSs can then be handled along with the PSs as part of a common time-series analyses (i.e., PS/DS solution), significantly improving point measurement density [20]. Recently, algorithms for performing multi-temporal interferometric analysis have been seamlessly integrated into cloud platforms, providing users with operational and automated services. This integration significantly reduces the need for extensive data storage, computational resources, and specialized expertise in executing complex processing chains. An example of such a service is the surface motion mapping (SNAPPING) service integrated on the Geohazards Exploitation Platform (GEP). SNAPPING is a PSI chain designed specifically for the Copernicus Sentinel-1 mission, capable of generating average motion and corresponding displacement time-series at various spatial resolutions.

The availability of PSI datasets at different resolutions provides the opportunity to initially investigate wide study areas, followed by subsequent detailed inspection. This configuration has been proven effective for covering wide areas at low cost, before focusing on a more thorough examination of particular areas or infrastructures [20].

From another perspective, the availability and accessibility of both PS and DS interferometric measurements present a unique challenge in regards to investigating suitable visualization methods. The spatial and temporal complexity of these data cannot be represented through traditional cartography techniques, thus necessitating innovative generalization and visualization methods.

Generalization is the process of meaningfully abstracting the infinite complexity and diversity found in the real world into a single, targeted cartographic representation that is usable and useful for the given map scale and purpose [21]. Generalization has been proven necessary when visualizing geospatial data among different cartographic scales [22]. When referring to point data generalization, different approaches have been established, such as aggregation, elimination, etc. [23]. F. Topfer [24] established a cartographic law that indicates the number of units that should be depicted on each cartographic map scale. All these approaches for point generalization are mostly based on the number of remaining points of a specific area of interest and not on the spatial distribution nor the significance of the points [25]. Therefore, a point generalization algorithm is proposed, which relies on the creation of grids and the calculation of spatial means for the points contained within each grid cell.

The interactivity of web applications offers dynamic approaches for spatial data analysis [26,27]. In exploring suitable and innovative visualization methods of PSI measurements, cartographic web applications have emerged as an essential medium for disseminating geospatial information [2]. Developing and utilizing web mapping applications offers

efficient ways of interacting with and presenting spatial data to the general public and domain experts [28–30]. Additionally, the necessity of user-friendly, interactive, open-source cartographic applications that can properly visualize any generic PSI dataset is evident [31,32]. This kind of cartographic web map application offers users the flexibility to interactively explore and analyze deformation rates and time-series deformation of specific areas of interest.

Several online platforms visualizing multi-temporal interferometric datasets have been released in recent past. The above fact underlines the necessity of such platforms in support of user exploitation of interferometric measurements. The most pronounced web interface is of the European Ground Motion Service (EGMS), handling vast amounts of data covering the European territory [33,34]. The EGMS interactive web map application plots mean velocities combined with time-series graphs, whereby the capability for 3D viewing is available. Automatic scaling of the size of the points based on the zoom level to avoid overlaps is also considered. An early version of such a web interface is the Norwegian Ground Motion Service, released by the Geological Survey of Norway (NGU), the Norwegian Water Resources and Energy Directorate (NVE), and the Norwegian Space Center (NSC) in November 2018. Ground Movement Service Germany (BBD) [35] is an online interactive platform exhibiting interferometric data covering Germany. Four different products with standard resolution are currently being visualized. Velocity rates and time-series of displacements are visualized via the platform. The Dutch Ground Motion Service [36] is a platform developed by the Netherlands Center for Geodesy and Geo-Informatics (NCG), in collaboration with knowledge centers, geodetic businesses, and universities. The platform visualizes ground motion datasets covering the Netherlands, Belgium, and Luxembourg. Mean velocity and time-series graphs are visualized for over 200 million point measurements. For small cartographic scales, a pixel-based approach is applied, where measurements are presented as squares measuring 300 × 300 m, whereas for large cartographic scales, the measurements are presented as individual points. The IREA-CNR InSAR web GIS [37] is an online platform visualizing individual SBAS datasets in specific locations around the world. When zooming to a specific area of interest, ground deformation data for mean velocity are presented, in combination with time series deformation values. Targets are visualized as hollow circles/ring shapes, with their perimeter color based on the mean velocity of deformation. For the above cases, overlaps between neighboring point measurements occur at small cartographic scales or at a reduction of point density, based on the fact that a regularly distributed grid is considered.

In this context, the present article introduces a novel approach to address the challenges of visualizing PSI datasets of different resolutions in predefined cartographic scales. Generalizing PSI datasets of different resolutions in different pre-defined cartographic scales, based on cartographic criteria, enhances the avoidance of overlapping PSs. For each PSI dataset, one appropriate cartographic scale fulfills the need for proper visualization. Visualizing PSI datasets in smaller cartographic scales, the density of points imposes cartographic challenges due to overlapping points. Hence, generalization of such data is required for appropriate visualization. For each one of those cartographic scales, generalized PSI datasets consisting of both original points (in areas with an acceptable density of targets) and newly created points (in areas with a high density of targets where overlapping occurs) are used for visualization. For less-experienced users, a web application is developed, providing scale-based generalization to each generic PSI dataset. All the above, combined with interactive web tools, such as data filtering and graph plots served by a cartographic web map application, offer users invaluable insights into intricate geospatial information, based on which informed decisions can be made.

2. Study Area

The study area is Lesvos Island (Figure 1). With a total area of 1632 km^2, Lesvos is the third-largest Greek island, located in the northeastern Aegean Sea. According to the 2021 census, there are 83,755 inhabitants on the island, whereas 33,523 people live in Mytilene,

the capital city. Two gulfs, the larger Kalloni Gulf in the west and the smaller Gera Gulf in the east, divide the island into three parts. Mount Lepetimnos (968 m) and Mount Olympus (968 m) are the two highest mountains on the island. From a geological standpoint, Lesvos consists of Alpine and pre-Alpine rocks that were later covered by post-Alpine formations, primarily Miocene volcanic rocks and Neogene marine and lacustrine deposits [38].

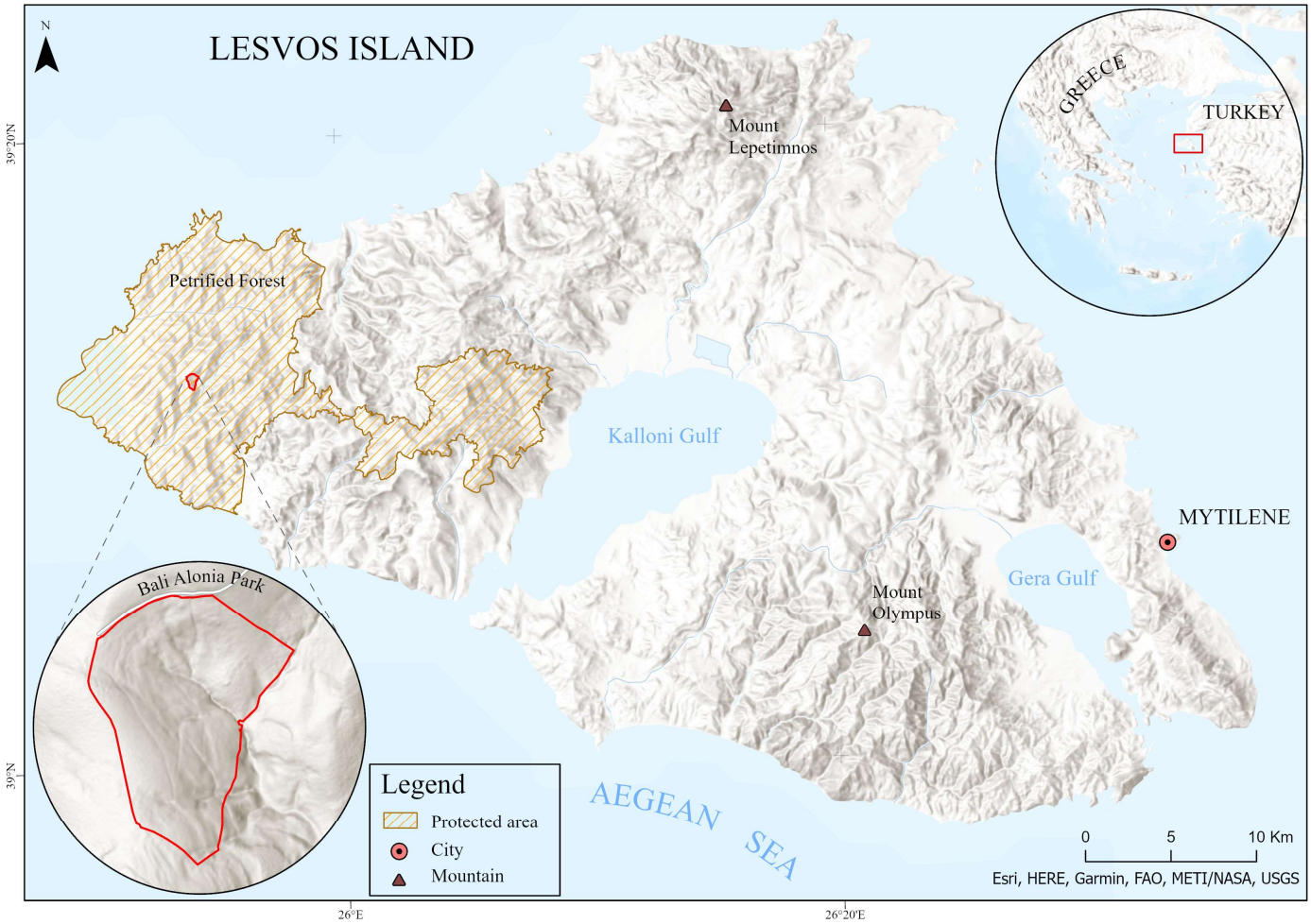

Figure 1. Area of interest (Lesvos Island) in the NE part of Greece, and Bali Alonia Park, on the W part of the island. Base map sources: Esri, Here, Garmin, FAO, METI/NASA, USGS.

Climate is typified by significant seasonal and regional changes in rainfall, as well as significant oscillations between daily minimum and maximum temperatures, both of which are typical of the Mediterranean region. The average annual rainfall ranges from 677 mm in the eastern part of the island to 415 mm in the western part, indicating a gradient in rainfall across the island. The mean annual air temperature of the island is 17.7 °C [39]. Lesvos' topography is mainly uneven, with steep hillsides that encourage the growth of runoff and erosion. The majority of the island is characterized as fragile or critical to desertification, where only 3.6% of the area is not affected by desertification [40].

Lesvos Island is characterized by numerous geological sites, areas of natural beauty, a rich biotic and abiotic heritage, and numerous cultural monuments [41]. Therefore, it is recognized as a UNESCO Global Geopark. Geological structures like volcanoes, fossil sites, active faults, waterfalls, and hot springs may be found all around Lesvos Island [42]. The Petrified Forest of Lesvos, which is located on the western peninsula of the island, is the most well-known geoheritage site on the island.

3. Materials and Methods

The methodology of this study is represented by the flowchart in Figure 2, and it consists of three main steps.

1. Data: Describing all the PSI datasets generated and the auxiliary data used for the needs of the current investigation, as well as for visualization.
2. Cartographic scales: Investigation of visualization parameters for multiscale PSI generalization, using tailored cartographic scales (color scheme, symbol size, etc.), following specific cartographic rules. Generalized datasets are joined with auxiliary data, based on their attributes, and are then utilized for database creation.
3. Geo-visualization: Web application development, contributing to the automation of the multiscale generalization of PSI datasets, while adhering to cartographic rules, as well as cartographic web map application development, contributing the appropriate visualization and investigation of PSI datasets at different cartographic scales.

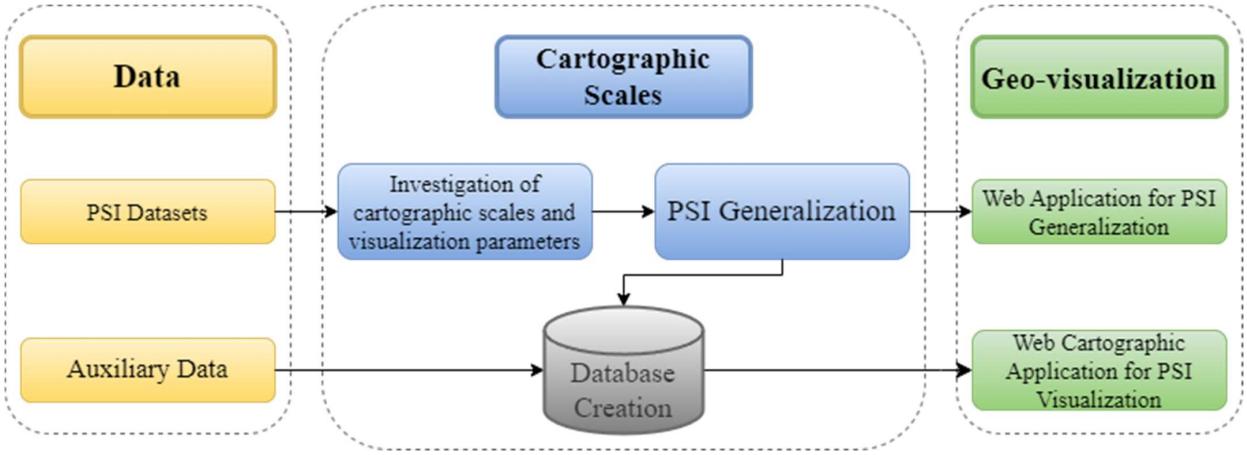

Figure 2. Overall workflow (flow chart).

3.1. Data

3.1.1. PSI Measurements

The processing of Sentinel-1 SAR data is conducted via the SNAPPING service on GEP, where PSI services are offered at different spatial resolutions. Two different resolution datasets (PSI Med and PSI Full) were used for this study. SNAPPING provides three distinct services. The first one is the SNAPPING IFG, used for generating interferometric stacks. These stacks are subsequently used as input for the SNAPPING PSI Med (i) and SNAPPING PSI Full (ii) services, which perform PSI analyses at medium and full resolutions, respectively. The SNAPPING service also provides PSI time-series analysis service for both resolutions [20]. The PSI processing, focusing on (iii) PS/DS scatterers, was executed at the Aristotle University of Thessaloniki (AUTh), using its infrastructures, based on the SNAPPING IFG outputs, i.e., differential interferograms and auxiliary data previously generated on GEP. It is important to mention that common processing parameters were considered for the various solutions to maintain measurement consistency, while deviation due to different references were adjusted accordingly.

Based on specified criteria, detected persistent scatterer (PS) targets of the SNAPPING PSI Med dataset were initially merged over a 100 m search radius, reducing their numbers over areas with high point densities. For SNAPPING PSI Full, no merging of neighboring PS targets is considered, retaining the original sensor resolution. Compared to PS-InSAR, the results of DS-InSAR significantly increase the spatial distribution density of point targets, especially in areas with lower coherence [20].

PSI Med and Full resolution datasets consist of 45,749 and 283,419 PSs, respectively, geolocated in the broader area of Lesvos Island, for the period between 2015–2020. The

PS/DS dataset consists of 11,169 points for the period between 2019–2021 located in the broader area of Bali Alonia Park. When referring to dataset point density, for an area of 40 ha, the number of targets varies significantly between each dataset's resolution, as presented in Figure 3.

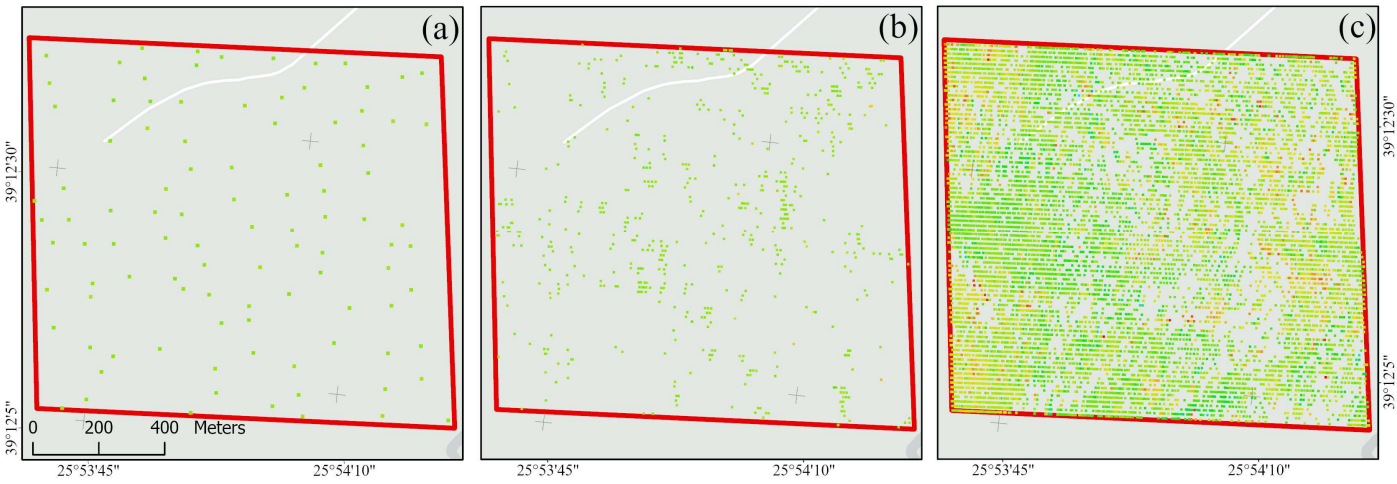

Figure 3. On the same area of 40 ha, different numbers of PSs are presented for each dataset, with 67 points for PSI Med (**a**), 267 points for PSI Full (**b**), and 2752 points for PS/DS (**c**) dataset located, respectively. Base map sources: Esri, TomTom, Garmin, Foursquare, GeoTechnologies, Inc, METI/NASA, USGS.

3.1.2. Auxiliary Data

Depending on each cartographic scale, PSI data are joined with auxiliary data to fulfil visualization requirements and to allow for improved exploitation. Combining PSI data with auxiliary data provides essential ground deformation details prevailing in specific infrastructures, like road networks, bridges, etc. [43]. The auxiliary data used consisted of:

- ESA Land Cover 2020 [44], at 10 m spatial resolution.
- Geology layer, consisting of two different datasets. The first one was digitized via the freely available geological map of Greece (1:500,000) of the Hellenic Geological and Mining Research Authority (E.A.G.M.E) [45]. The second one (1:50,000) was obtained through the Cartography and Geoinformatics Laboratory of the University of the Aegean.
- Road network data, as obtained via OpenStreetMap [46]. The road network was separated throughout various datasets, according to OSM's visualization for each cartographic scale.
- Minning, airport, and geosite data used were obtained from the Cartography and Geoinformatics Laboratory of the University of the Aegean.

3.2. Data Pre-Prosessing and PSI Generalization

3.2.1. Investigation of Cartographic Scales and Visualization Parameters

Based on previous studies [47,48], the need for PSI interpretation according to pre-specified scales arises. By combining the area that each PSI dataset covers with different geographic scales (regional scale, local scale, etc.), eight predefined cartographic scales are obtained:

1. 1:1,000,000
2. 1:500,000
3. 1:200,000
4. 1:100,000
5. 1:50,000
6. 1:20,000
7. 1:10,000
8. 1:5000

The need for upscaling and downscaling requires a linear ratio of transitions between the initial and desirable scales [25].

In terms of classifying quantitative data, persistent scatterer (PS) targets are suggested to be visualized using a "stretch" method [47]. The color scale that is commonly used [47] is a color palette ranging from blue to red for indicating movements away and towards the satellite, respectively. The symbol size of the PSs should be adapted to each cartographic scale. It is widely acknowledged that cartographic representation is linked to visual acuity. In traditional cartography, the threshold ranges between 0.1 and 1.0 mm [49]. In web cartography, parameters such as screen resolution or the distance between the user and the screen indicate that visual acuity cannot be measured in a single manner, and that it varies from individual to individual. Nevertheless, the thresholds here vary between 0.4 and 0.6 mm for point data [50]. Herein, the combination of minimum thresholds for visualizing point data [51], along with a strict approach, allows for the minimum threshold for points presentation to be set to 0.25 mm. In any other case, the point symbol size can be larger in accordance with each cartographic scale and the point density of the data in order to fit the cartographic needs.

3.2.2. PSI Generalization Algorithm

When visualizing PSI datasets, the distribution and density of points leads to the undesirable overlapping of point measurements, especially when using small cartographic scales. The generalization of points is a cartographic technique that provides a reliable solution for proper visualization of the LoS (line of sight) displacements, but not for further data analysis. Eliminating or creating new points enhances the visual outcome, without affecting the distribution of the phenomenon. For larger cartographic scales, higher resolution PSI datasets should be used for visualization. If there is no availability of multiple resolution PSI datasets, a scale-based symbol size adjustment should be applied.

As a requirement for the current work, a generalization algorithm was developed for such points. Based on the visual acuity of the human eye in each predefined cartographic scale, eight grids with corresponding cell sizes were created, as presented in Table 1. The third column of the table indicates the PSI dataset used for each cartographic scale. The fourth column demonstrates the number of points visualized on each cartographic scale, after the generalization procedure. The fifth column refers to the point density for each one of the predefined cartographic scales.

Table 1. Predefined cartographic scales used for visualization, followed by the PSI dataset visualized in each case. For generalization needs, a grid was created for each cartographic scale, along with the corresponding cell size. For each cartographic scale, a dataset (either generalized or not) is generated with the corresponding number of points.

Cartographic Scale.	Cell Size (m)	PSI Dataset	No. of Points	Point Density (Points/km^2)
1:1,000,000	250	PSI Med	14,348	15
1:500,000	125	PSI Med	31,189	66
1:200,000	50	PSI Med	45,749	99
1:100,000	25	PSI Full	158,030	376
1:50,000	12.5	PSI Full	231,166	507
1:20,000	5	PSI Full	283,419	580
1:10,000	2.5	PS/DS	11,169	9422
1:5000	1.25	PS/DS	11,169	9422

A 250 m grid was applied to the lowest resolution PSI dataset (PSI Med) and the smallest predefined cartographic scale (1:1,000,000). For each cell containing only one PS target, no changes were applied, resulting in a subset of 4017 targets of the original dataset. For cells containing more than one PS target, a new point was created, located in the

spatial mean of the PSs contained in each cell. All other PSs of this cell were deleted. The velocity of each newly created point is calculated by averaging all PS velocities at the exact cell, resulting in a 10,331-point subset. The subsets of the original targets and the newly created points are merged. The generalized dataset, used for visualization in this specific cartographic scale, consists of 14,348 points. For the cartographic scale of 1:500,000, a 125 m grid was applied to the PSI Med dataset. There were 19,507 cells containing only one original target and 11,682 containing more than one. Consequently, 11,682 new points were created and merged with 19,507 original targets, forming a generalized dataset consisting of 31,189 points. For the cartographic scale of 1:200,000, a 50 m grid was applied to the PSI Med dataset. There were 41,050 cells containing one original target and 3090 cells containing more than one target. Following the same procedure, the generalized dataset consists of 44,749 points. Since the point count of the generalized dataset was higher than 85% of the original dataset's point count, the original dataset was used for this cartographic scale, as it is considered the most suitable for visualization.

The procedure was then repeated for the next available higher resolution PSI dataset, at the next larger predefined cartographic scale. For the cartographic scale of 1:100,000, a 25 m grid was applied to the PSI Full dataset. There were 89,980 cells containing one original target and 68,050 cells containing more than one. The generalized dataset consisted of a total of 158,030 points (89,980 original targets and 68,050 newly created points). For the cartographic scale of 1:50,000, a 12.5 m grid was applied to the PSI Full dataset. There were 184,595 cells containing one original target and 46,571 cells containing more than one. The generalized datasets consisted of 231,166 points, of which 184,595 were derived from the original dataset, and 46,571 were newly created. For the cartographic scale of 1:20,000, a 5 m grid was applied to the PSI Full dataset, following the same procedure. The generalized dataset consisted of 273,434 points (262,867 original targets and 10,576 newly created points). Since this point count was higher than 85% of the original dataset's point count, the original dataset was used for visualization in this cartographic scale.

For cartographic scales 1:10,000 and 1:5000, grids of 2.5 m and 1.25 m were applied correspondingly to the PS/DS dataset. Each created cell contained only one original target; thus, no generalization was applied, and the original dataset was used for visualization.

Densities of different generalized datasets are derived from the corresponding grid size of each cartographic scale. In contrast, the densities of the original datasets derive from the corresponding service processing. An example of this procedure is presented in Figure 4.

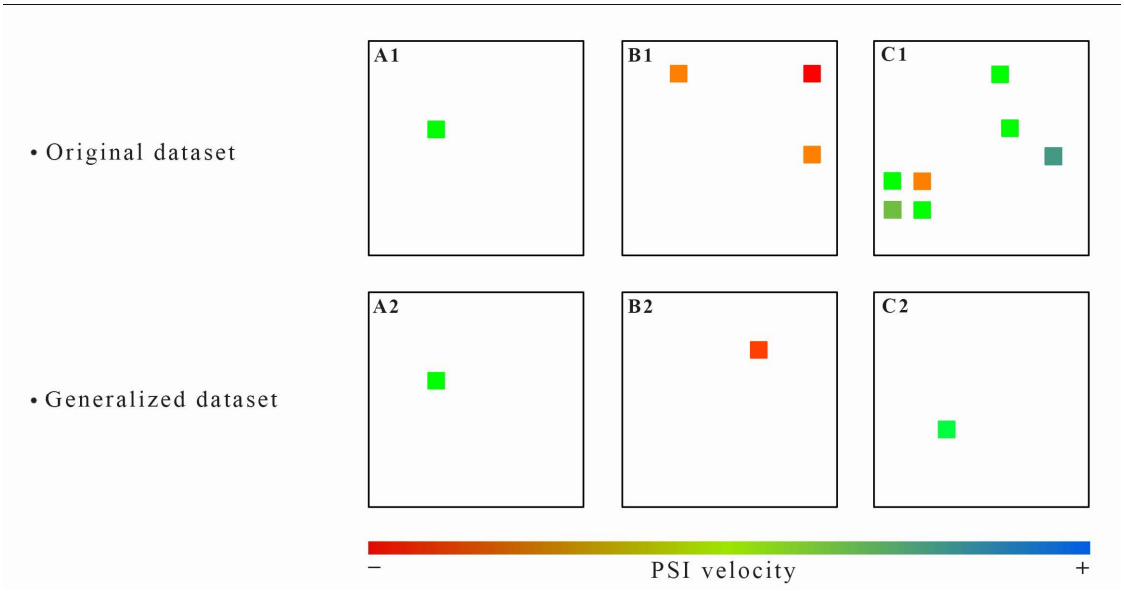

Figure 4. Random cells affected by the designed generalization procedure. Example A presents a cell containing a single PS target (**A1**), so no generalization is considered (**A2**). Examples B and C indicate

cells with 3 (**B1**) and 7 (**C1**) PSs from the original dataset. The corresponding spatial mean of each cell containing points of the original dataset is a newly created point for the generalized dataset ((**B2**,**C2**) respectively). The velocity rate of generalized dataset points (**B2**,**C2**) is the mean value of all containing point velocities for the corresponding cell of the original dataset (**B1**,**C1**), respectively.

The above-mentioned generalization algorithm is presented schematically in Figure 5. Figure 6 presents the PSI datasets used for each cartographic scale and the number of points generated after every generalization step. An example of a generalized map in a scale of 1:1,000,000, with a medium resolution PSI dataset, is presented in Figure 7.

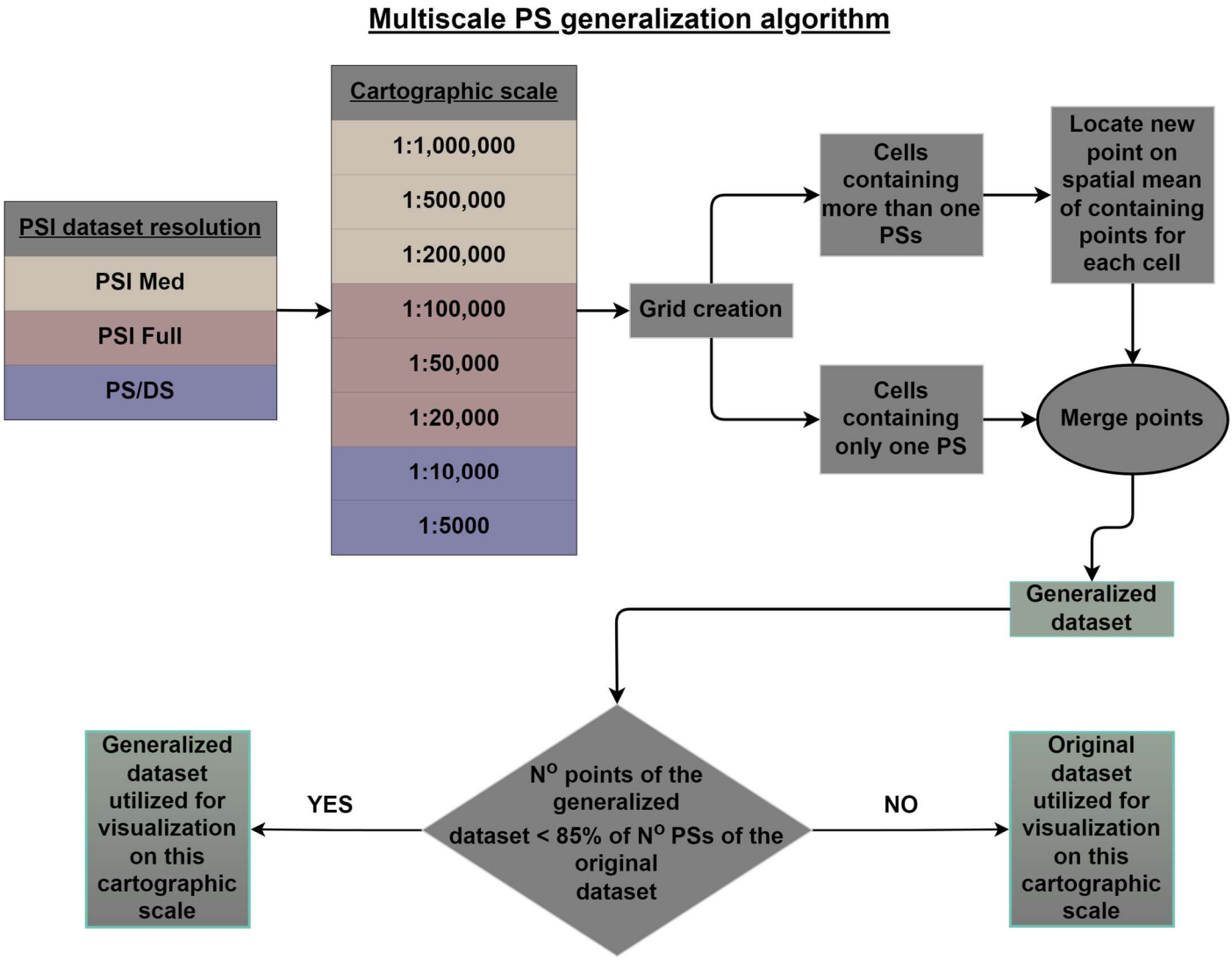

Figure 5. Flowchart of a generalization algorithm for PSI datasets of different resolutions are presented at various cartographic scales. The relationship between the PSI dataset resolution and the cartographic scales is presented using colors, as is the case for Figure 6 as well.

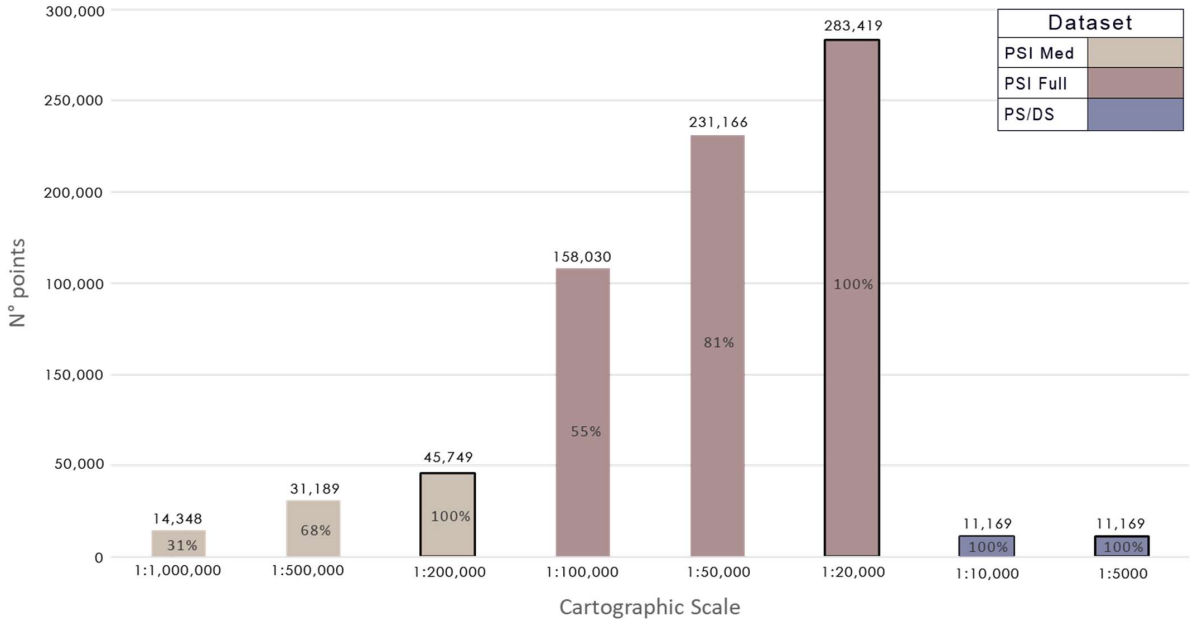

Figure 6. Dataset used for generalization of the smaller cartographic scale (1:1,000,000), consisting of 14,348 points (31% of the original dataset's point count, PSI Med). For the 1:500,000 scale, the generalized dataset used consists of 31,189 points (68% of the total number of points in the original dataset, PSI Med). For the 1:200,000 scale, the original dataset (45,749 points) is used. For the 1:100,000 scale, a generalized dataset consisting of 158,030 points (55% of the original dataset, PSI Full), is used. For the 1:50,000 scale, a generalized dataset of 231,166 points (81% of the total number of points in the original dataset, PSI Full), is used. For the 1:200,000 scale, the original PSI Full resolution of 283,419 points is used for visualization. For both the 1:10,000 and 1:5000 scales, the original PS/DS dataset is used for visualization. The columns with black boundaries indicate cartographic scales with no generalization requirements, which are considered to be the most suitable cartographic scales for each one of the original datasets.

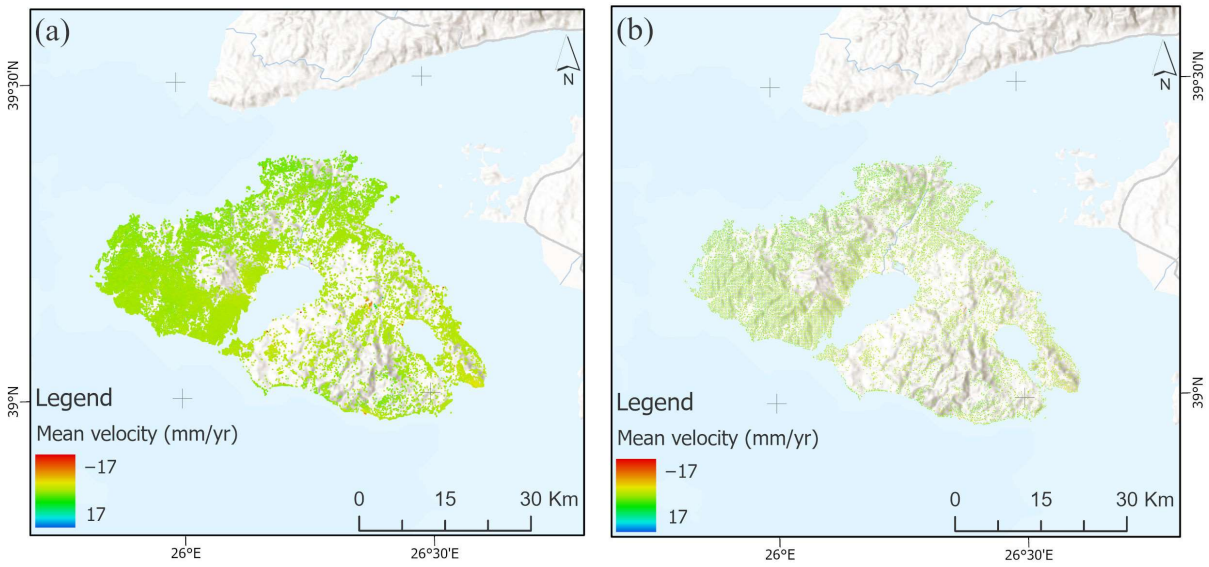

Figure 7. Generalization example of a map on a scale of 1:1,000,000. Generalization of PSs is based on a 250 m grid, and both datasets are visualized using the same symbol size for the point symbols. The original dataset consists of 45,749 points (**a**), whereas the generalized dataset consists of 14,348 points (**b**). From red (subsidence) to blue (uplift), colors indicate mean LoS displacement rates ranging from −17 up to 17 mm/year, respectively. Base map sources: Esri, HERE, Garmin, Foursquare, FAO, METIN/NASA, USGS.

After PS generalization, the symbol size and color scheme were adjusted according to the laws of cartography [25]. Based on all those available data, a database was created and uploaded to a server using ArcGIS Enterprise™. The following steps involved the creation of a detailed multiscale web map comprising all available PSI datasets. The exploitation of this web map, in combination with other useful cartographic tools, resulted in the development of a cartographic web map application.

4. Results

4.1. Target Points Generalization

Aiming at proper visualization, four generalized datasets were generated: two at medium resolution (on scales 1:1,000,000 and 1:500,000, respectively) and two at full resolution (on scales 1:100,000 and 1:50,000, respectively). For further investigation of the modification after the generalization of each created dataset, Table 2 presents the number of points that remain in the exact same location (original point targets), when compared to the original dataset, as well as their proportion. The distribution of original points in the generalized datasets is considered balanced, except for the one derived by the lowest resolution dataset (medium) on a smaller cartographic scale (1:1,000,000). Areas where the original dataset is characterized by a high density of points result in a lack of original points in the generalized dataset (i.e., the SW of Lesvos Island). The generalization algorithm was also applied to a medium resolution PSI dataset in the broader area of Thessaloniki for testing purposes. The results indicated similar percentages of stable points on both cartographic scales (35.5% for 1:1,000,000 and 63.5% for 1:500,000). For the cartographic scale of 1:500,000, the distribution of original targets was also normal. However, at the scale of 1:1,000,000, a deficiency of original targets of the generalized dataset is observed in areas where the original dataset is characterized by a high density of PSs.

Table 2. Predefined cartographic scales with the corresponding number of points that constitute each generalized dataset used for visualization. The third and fourth columns indicate the number of original PSs targets that remain in the exact same location after generalization, as well as their proportion, respectively.

Cartographic Scale	No. of Points of Generalized Dataset	No. of Original PSs of the Generalized Dataset	Percentage of Original PSs of the Generalized Dataset
1:1,000,000	14,348	4017	28%
1:500,000	31,189	19,507	62.5%
1:100,000	158,030	89,980	57%
1:50,000	231,166	184,595	80%

4.2. Web Applications

4.2.1. Web Cartographic Application for PSI Visualization

An interactive cartographic web application was developed, in which users have the option to properly visualize, explore, analyze, and export PSI data in each of the eight available cartographic scales. This application provides the layer list and legends of each dataset, according to each cartographic scale. Apart from changing the base map using a dropdown menu of available layers, other tools are also available to measure distances and areas. A preview of the web application is presented in Figure 8.

An additional feature included in the web application is the filtering tool. This tool allows for the filtering of points by their attributes, such as velocity, land cover, geology, road network proximity, etc. (described in Section 3.1.1). These attributes vary in each dataset, depending on the cartographic scale. For example, filtering the proximity of points to an airport is only available in large cartographic scales such as 1:50,000 or 1:20,000. Upon applying a specific filter rule, only the points that adhere to the defined criteria are displayed

on the screen. Finally, users have the option to select points to export, as more lightweight subsets in the ESRI Shapefile format. An example of this tool is shown in Figure 9.

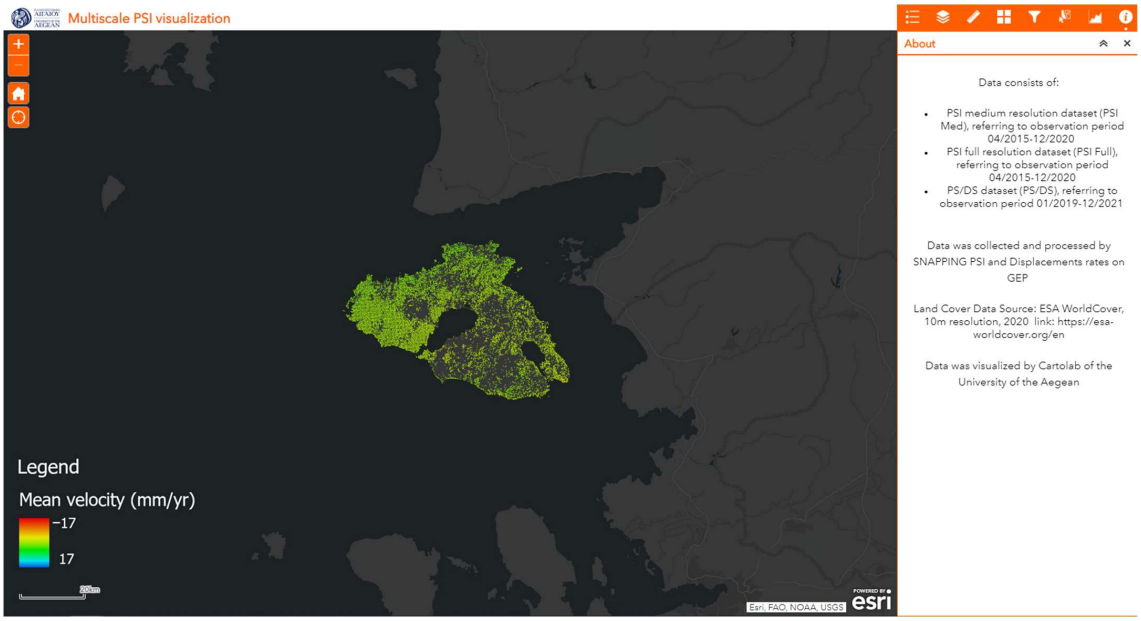

Figure 8. A preview of the cartographic web map application, presenting mean velocity rates of a PSI medium resolution dataset for Lesvos Island, generalized for a 1:1,000,000 scale presentation. From red (subsidence) to blue (uplift), colors indicate mean LoS displacement rates, ranging from −17 up to 17 mm/year, respectively. Base map sources: Esri, HERE, Garmin, Foursquare, FAO, METIN/NASA, USGS.

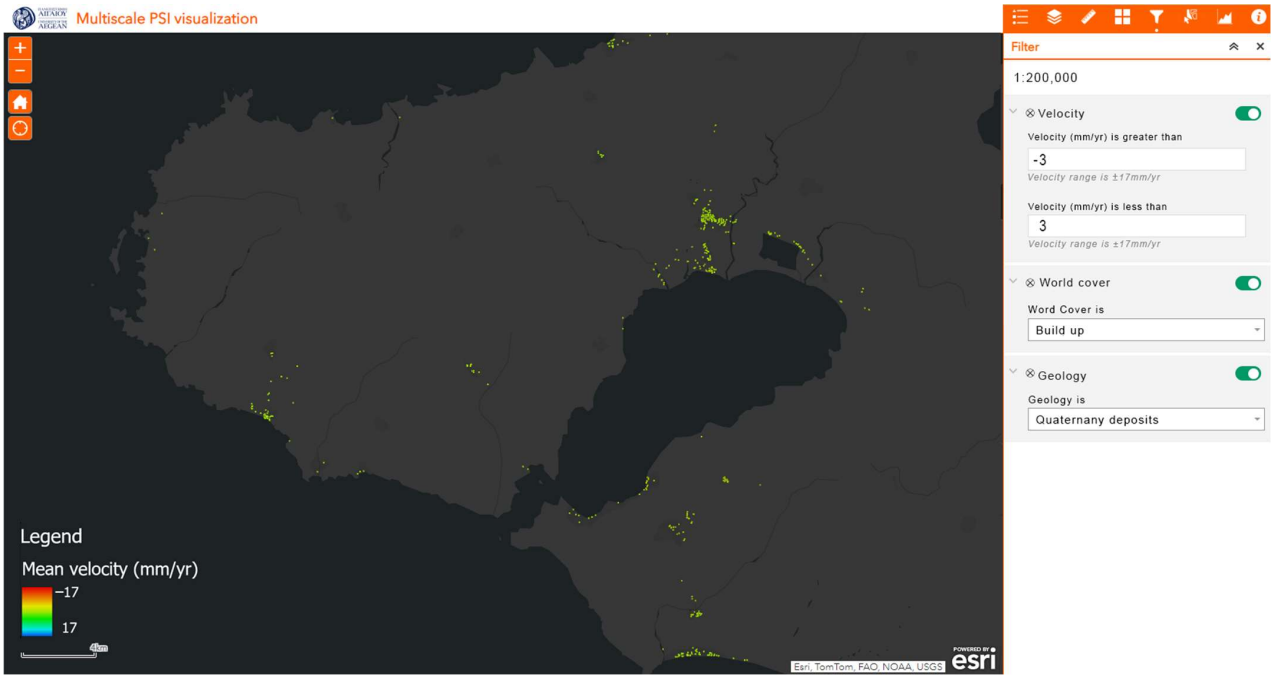

Figure 9. Mean velocity rates (mm/yr) from 2015–2020 for the west part of Lesvos Island. The PSI dataset refers to PSI Med resolution, at a scale of 1:200,000. Depicted PSs refer to the mean velocity, from −3 mm/yr to 3 mm/yr (with the corresponding color palette), located in quaternary deposits over built-up areas. Base map sources: Esri, HERE, Garmin, Foursquare, FAO, METIN/NASA, USGS.

Another tool added to the designed application is the graph plot. When generalizing datasets, points are spatially reduced, based on the defined cartographic scale. Time-series analysis is not applicable in generalized data, due to a limitation related to the calculation of the average velocity of each newly created point. To compensate for this limitation, the time-series graph is only generated for the original data at their identical cartographic scale. By using the graph tool, users can select the original dataset needed and then select a point for which the time-series deformation graph will be generated. This also allows users to investigate, in graph form, not only the mean velocity, but also the evolution of ground motion over time. An example of this tool is presented in Figure 10.

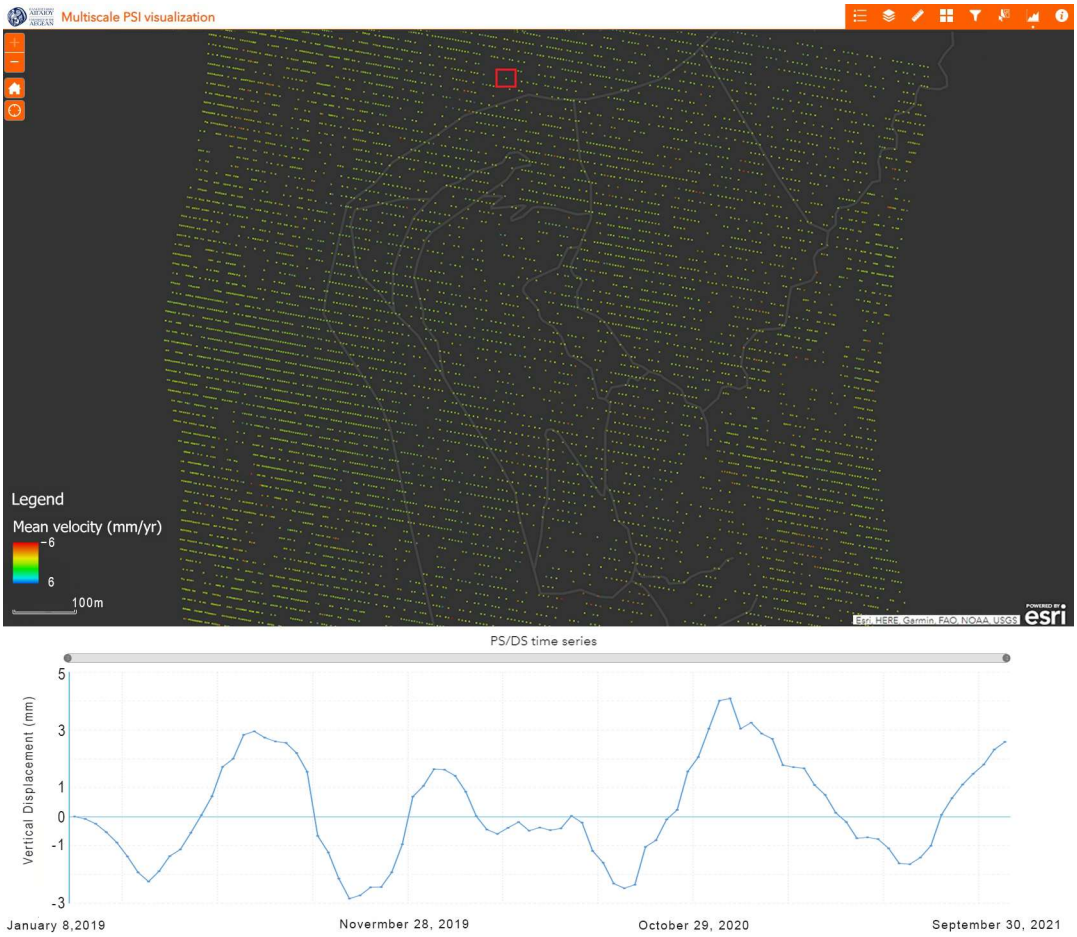

Figure 10. An example of a generated graph presenting the displacement time-series of a selected target. The dataset depicted is a PS/DS dataset at a 1:5000 scale, from red (subsidence) to blue (uplift); colors indicate mean LoS displacement rates ranging from −6 up to 6 mm/year, respectively. The point selected for graph creation is the one in the red square, on the north side of Bali Alonia Park. The plot presents the LoS displacements from January 2019 to September 2021. Base map sources: Esri, HERE, Garmin, Foursquare, FAO, METIN/NASA, USGS.

This web cartographic application is accessible using the following link: https://sdi-portal.aegean.gr/PSIMultiscaleVisualizationWebApplication or PSI Multiscale Visualization Web Application PSI Multiscale Visualization Web Application (accessed on 13 February 2024 https://sdi-portal.aegean.gr/portal/apps/webappviewer/index.html?id=da2ee539746647b9890290b325052e39).

4.2.2. Web Application for PSI Generalization

For automating the PSI generalization procedure, a web application including a graphical user interface was developed, utilizing the R programming language and the R Shiny

web interface. Users can upload any PSI dataset, and after selecting the necessary details (variables and cartographic scale), the generalization algorithm (described in Section 3.2.2) is applied, making it possible to download the results in an interchangeable format for later use. When the resulting dataset consists of more than 85% of the points from the original dataset, a notification pops up, informing users that there is no need for the generalization of points at such a cartographic scale. The integration of the R programming language into the web environment offers the flexibility of applying complex spatial analysis procedures on the web interface, without the need for complex scripts and methods. Generally, this web application will facilitate points generalization for the user, without the need to locally install any other software or additional specialized libraries. This web application is accessible using the following link: http://sagisrs.MultiscalePSIGeneralizationWebApplication or Multiscale PSI Generalization Web Application Multiscale PSI Generalization Web Application (accessed on 13 February 2024). An example of the web application is presented in Figure 11.

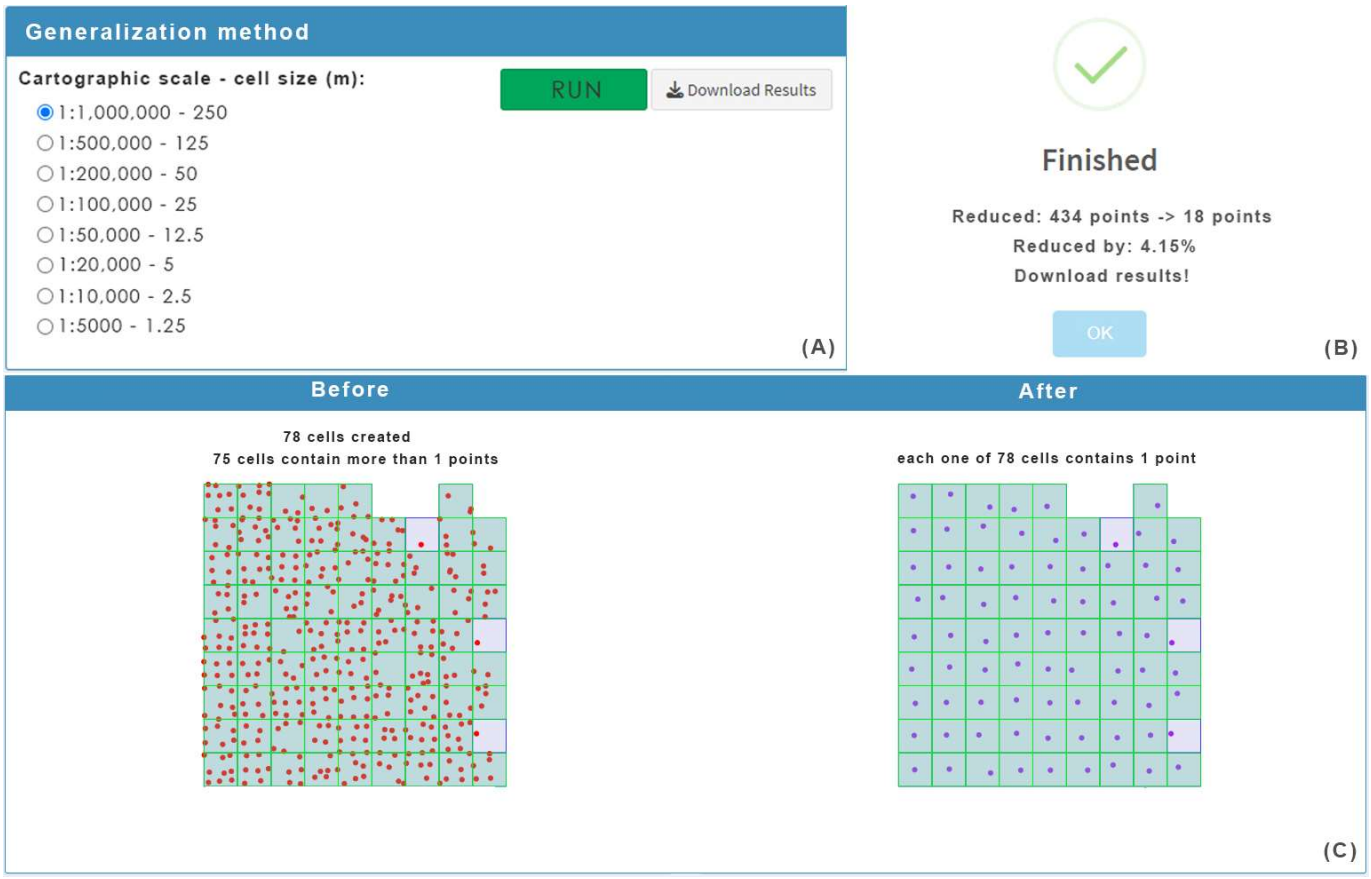

Figure 11. A preview of the web application for PS target generalization. (**A**) A generic PSI dataset, consisting of 434 point targets, is generalized at a scale of 1:1,000,000. (**B**) Pop-up message after generalization procedure. For a generalized dataset consisting of 18 points, the number of points is reduced by 4.15% compared to the number in the original dataset. (**C**) Preview of both (original and generalized) datasets. The transparent cells contain the original PSs. A download option is available for the generalized dataset.

5. Discussion

To address the requirement for the proper multiscale visualization of PSI data, a cartographic web map application was developed. This web application allows for both the visualization and exploitation of PSI motion rates, in detail. Any PSI dataset, after proper processing, can be tailored and further explored by using the proposed cartographic

web map application. Its design and functionalities support the geographic, cartographic, spatial, and temporal investigation of PSI datasets with different resolutions.

The limitations mainly come from the significant challenge of the management and processing of PSI datasets containing large numbers of point records. Generalizing and visualizing such data can prove to be significantly demanding in terms of computational power and time requirements. Another limitation arises from the web application development procedure. Specific cartographic tools are provided, requiring relevant adjustment, in order to provide users with interactive data exploitation.

Additionally, the analysis of PSI displacement time-series via a graph tool is also supported. The specific tool is applicable only to the original datasets, where no generalization is considered. Further tools involve point filtering based on the location and attributes of the points. Any available auxiliary data, after proper ingestion, could be used in order to update the filtering parameters of the points, according to user needs.

The implemented multiscale geo-visualization of PS targets remains a time-consuming process, especially for large datasets, although the generalization method considered in this study can be easily applied within common GIS packages. For less-technically savvy users, a graphical user interface (GUI), in which users only need to load any PSI dataset and determine the preferred visualization scale, can improve their experience regarding the utilization of these complex measurements. This is an advantage, as users from different domains benefit from such a generalization approach simply by accessing the web-application, which also supports a data download option. Such a web-based application also reduces the installation requirements, due to its cross platform compatibility and centralized future upgrades.

Often, low resolution PSI datasets are meant for the analysis of wide areas, whereas higher spatial resolution datasets are typically generated for a detailed investigation over smaller areas of interest. Therefore, this approach is advisable, as it requires fewer processing resources. Although a scale-based visualization approach can be achieved with a single, maximum (higher density) resolution dataset generalized at large cartographic scales, a multiscale visualization platform is proposed, based on the availability of different resolution datasets.

When no generalization of a PSI dataset is needed for a particular cartographic scale, then this scale is the most appropriate option for visualization purposes. This study shows that for a medium resolution PSI dataset, the most significant cartographic scale for visualization is 1:200,000, while for the full sensor resolution datasets, based on Copernicus Sentinel-1 mission data, the most appropriate scale is 1:20,000. For a PS/DS dataset with a higher point density, optimum visualization, without the need for generalization, is at a scale of 1:10,000.

When generalizing PSI datasets, the highest proportion of newly created points is presented at a smaller cartographic scale (1:1,000,000), as when visualizing a subset originating from a medium resolution dataset. In this case, these depicted areas are mostly characterized by a high density of targets from the original dataset. For each of the remaining subsets generated (referring to each remaining cartographic scale), the proportions of the newly created points average about 67%, while the remaining points constitute the original targets. Newly created points exhibit a normal distribution across the study area. Thus, there is a need for proper visualization of PSs via generalization, especially at smaller cartographic scales.

6. Conclusions

The combination of the aforementioned cartographic geo-visualization tools and methods leads to effective multiscale exploitation of various PSI datasets, providing easier extraction of ground motion information.

Generalized PSI datasets enhance the proper visualization of measurements at different cartographic scales, supporting qualitative data exploitation. Each original PSI dataset is optimally visualized at a specific cartographic scale, determined by the dataset's point density. Visualizing original datasets at corresponding optimal cartographic scales not

only facilitates the proper depiction of ground displacement, but also facilitates both the qualitative and quantitative spatiotemporal analysis of the original targets, such as through the generation of time-series graphs.

By visualizing PSI datasets at appropriate cartographic scales via the web map application, it is clearly shown that Lesvos Island is not characterized by significant ground deformation. Negative velocity rates between −5 mm/yr and −8 mm/yr, indicating land subsidence, are derived in the east part of the island, close to Lampou Mili village. Positive velocity rates (i.e., uplift) reaching 2 mm/yr, are noted on the northern part of the island, between the Mythimna–Efthalou region.

Through this work, we aim to contribute to the enhanced visualization and exploitation of PSI datasets in support of EO practitioners by presenting a new and effective solution to PSI data visualization, ultimately enhancing the exploitation of these valuable measurements. Future research is mainly oriented towards adopting the web map application for the efficient management of big EO data, such as nationwide PSI, and enriching the collection of cartographic tools. This will lead to the development of a less resource-demanding web application, where users can upload any PSI dataset for appropriate visualization. The adoption of such a generalization application by existing EO platforms would facilitate the advanced visualization of PSI measurements for a wider range of users.

Author Contributions: Conceptualization, Panagiotis Kalaitzis, Michael Foumelis and Nikolaos Soulakellis; methodology, Panagiotis Kalaitzis, Michael Foumelis, Antonios Mouratidis, Dimitris Kavroudakis and Nikolaos Soulakellis; investigation, Panagiotis Kalaitzis; data curation, Michael Foumelis; writing—original draft preparation, Panagiotis Kalaitzis, Michael Foumelis and Dimitris Kavroudakis; writing—review and editing, Michael Foumelis, Antonios Mouratidis and Nikolaos Soulakellis; visualization, Panagiotis Kalaitzis; supervision, Michael Foumelis, Antonios Mouratidis, Dimitris Kavroudakis and Nikolaos Soulakellis. All authors have read and agreed to the published version of the manuscript.

Funding: This research received no external funding.

Data Availability Statement: The original contributions presented in the study are included in the article, further inquiries can be directed to the corresponding author.

Conflicts of Interest: The authors declare no conflict of interest.

References

1. Gehlot, S.; Hanssen, R.F. Monitoring and Interpretation of Urban Land Subsidence Using Radar Interferometric Time Series and Multi-Source GIS Database. In *Remote Sensing and GIS Technologies for Monitoring and Prediction of Disasters*; Springer: Berlin/Heidelberg, Germany, 2008; pp. 137–148.
2. Kraak, M.-J.; Ormeling, F. *Cartography: Visualization of Geospatial Data*; CRC Press: Boca Raton, FL, USA, 2020.
3. Crosetto, M.; Monserrat, O.; Cuevas-González, M.; Devanthéry, N.; Crippa, B. Persistent Scatterer Interferometry: A Review. *ISPRS J. Photogramm. Remote Sens.* **2016**, *115*, 78–89. [CrossRef]
4. Ao, M.; Wang, C.; Xie, R.; Zhang, X.; Hu, J.; Du, Y.; Li, Z.; Zhu, J.; Dai, W.; Kuang, C. Monitoring the Land Subsidence with Persistent Scatterer Interferometry in Nansha District, Guangdong, China. *Nat. Hazards* **2015**, *75*, 2947–2964. [CrossRef]
5. Aslan, G.; Foumelis, M.; Raucoules, D.; De Michele, M.; Bernardie, S.; Cakir, Z. Landslide Mapping and Monitoring Using Persistent Scatterer Interferometry (PSI) Technique in the French Alps. *Remote Sens.* **2020**, *12*, 1305. [CrossRef]
6. Crosetto, M.; Monserrat, O.; Jungner, A.; Crippa, B. Persistent Scatterer Interferometry: Potential and Limits. In Proceedings of the Proceedings of the 2009 ISPRS Workshop on High-Resolution Earth Imaging for Geospatial Information, Hannover, Germany, 2–5 June 2009; Volume 25.
7. Mouratidis, A.; Costantini, F.; Votsis, A. Correlation of DInSAR Deformation Results and Active Tectonics in the City of Thessaloniki (Greece). In Proceedings of the 2011 Joint Urban Remote Sensing Event, Munich, Germany, 11–13 April 2011; pp. 421–424.
8. Ferretti, A.; Fumagalli, A.; Novali, F.; Prati, C.; Rocca, F.; Rucci, A. A New Algorithm for Processing Interferometric Data-Stacks: SqueeSAR. IEEE Trans. Geosci. *Remote Sens.* **2011**, *49*, 3460–3470. [CrossRef]
9. Papageorgiou, E.; Foumelis, M.; Trasatti, E.; Ventura, G.; Raucoules, D.; Mouratidis, A. Multi-Sensor SAR Geodetic Imaging and Modelling of Santorini Volcano Post-Unrest Response. *Remote Sens.* **2019**, *11*, 259. [CrossRef]
10. Chen, Y.; Li, J.; Li, H.; Gao, Y.; Li, S.; Chen, S.; Guo, G.; Wang, F.; Zhao, D.; Zhang, K.; et al. Revealing Land Surface Deformation Over the Yineng Backfilling Mining Area, China, by Integrating Distributed Scatterer SAR Interferometry and a Mining Subsidence Model. *IEEE J. Sel. Top. Appl. Earth Obs. Remote Sens.* **2023**, *16*, 3611–3634. [CrossRef]

11. Caprino, A.; Puliero, S.; Lorenzoni, F.; Floris, M.; da Porto, F. Satellite SAR Interferometry and On-Site Traditional SHM to Monitor the Post-Earthquake Behavior of the Civic Tower in L'Aquila (Abruzzo Region, Italy). *Remote Sens.* **2023**, *15*, 1587. [CrossRef]
12. Shin, Y.; Lee, H. Subsidence of a Coal Ash Landfill in a Power Plant Observed by Applying PSInSAR to Sentinel-1 SAR Data. *Remote Sens.* **2023**, *15*, 4127. [CrossRef]
13. Costantini, F.; Mouratidis, A.; Schiavon, G.; Sarti, F. Advanced InSAR Techniques for Deformation Studies and for Simulating the PS-Assisted Calibration Procedure of Sentinel-1 Data: Case Study from Thessaloniki (Greece), Based on the Envisat/ASAR Archive. *Int. J. Remote Sens.* **2016**, *37*, 729–744. [CrossRef]
14. Singh, H.; Pandey, A.C. Land Deformation Monitoring Using Optical Remote Sensing and PS-InSAR Technique Nearby Gangotri Glacier in Higher Himalayas. *Model. Earth Syst. Environ.* **2021**, *7*, 221–233. [CrossRef]
15. Nahli, A.; Simonetto, E.; Tatin, M.; Durand, S.; Morel, L.; Lamour, V. On the combination of psinsar and gnss techniques for long-term bridge monitoring. *Int. Arch. Photogramm. Remote Sens. Spat. Inf. Sci.* **2020**, *43*, 325–332. [CrossRef]
16. Parwata, I.N.S.; Osawa, T. Surface Deformation Monitoring Induced by Volcanic Activity of Mount Agung, Indonesia, by PS-InSAR Using Sentinel-1 SAR from 2014–2021. In Proceedings of the 2021 7th Asia-Pacific Conference on Synthetic Aperture Radar (APSAR), Bali Island, Indonesia, 15 November 2021; pp. 1–4.
17. Ho Tong Minh, D.; Ngo, Y.-N. Compressed SAR Interferometry in the Big Data Era. *Remote Sens.* **2022**, *14*, 390. [CrossRef]
18. Even, M.; Schulz, K. InSAR Deformation Analysis with Distributed Scatterers: A Review Complemented by New Advances. *Remote Sens.* **2018**, *10*, 744. [CrossRef]
19. Li, Y.; Zuo, X.; Yang, F.; Bu, J.; Wu, W.; Liu, X. Effectiveness Evaluation of DS-InSAR Method Fused PS Points in Surface Deformation Monitoring: A Case Study of Hongta District, Yuxi City, China. *Geomat. Nat. Hazards Risk* **2023**, *14*, 2176011. [CrossRef]
20. Foumelis, M.; Delgado Blasco, J.M.; Brito, F.; Pacini, F.; Papageorgiou, E.; Pishehvar, P.; Bally, P. SNAPPING Services on the Geohazards Exploitation Platform for Copernicus Sentinel-1 Surface Motion Mapping. *Remote Sens.* **2022**, *14*, 6075. [CrossRef]
21. Müller, J.C.; Zeshen, W. Area-Patch Generalisation: A Competitive Approach. *Cartogr. J.* **1992**, *29*, 137–144. [CrossRef]
22. Raposo, P.; Touya, G.; Bereuter, P. A Change of Theme: The Role of Generalization in Thematic Mapping. *ISPRS Int. J. Geo-Inf.* **2020**, *9*, 371. [CrossRef]
23. Müller, J.C.; Weibel, R.; Lagrange, J.P.; Salgé, F.; Müller, J.C.; Lagrange, J.P.; Weibel, R. Generalization-State of the Art and Issues. In *GIS And Generalisation*; CRC Press: Boca Raton, FL, USA, 2020; pp. 3–17.
24. Töpfer, F.; Pillewizer, W. The Principles of Selection. *Cartogr. J.* **1966**, *3*, 10–16. [CrossRef]
25. Robinson, A.H.; Morrison, J.L.; Muehrcke, P.C.; Kimerling, A.J.; Guptill, S.C. *Elements of Cartography*, 6th ed.; John Willey Sons: New York, NY, USA, 1995; 544p.
26. Belussi, A.; Catania, B.; Clementini, E.; Ferrari, E. *Spatial Data on the Web: Modeling and Management*; Springer: Berlin/Heidelberg, Germany, 2007.
27. Becirspahic, L.; Karabegovic, A. Web Portals for Visualizing and Searching Spatial Data. In Proceedings of the 2015 38th International Convention on Information and Communication Technology, Electronics and Microelectronics (MIPRO), Opatija, Croatia, 25–29 May 2015; pp. 305–311.
28. Zerdoumi, S.; Hashem, I.A.T.; Jhanjhi, N.Z. A New Spatial Spherical Pattern Model into Interactive Cartography Pattern: Multi-Dimensional Data via Geostrategic Cluster. *Multimed. Tools Appl.* **2022**, *81*, 22903–22952. [CrossRef]
29. Yi, J.S.; Kang, Y.; Stasko, J.; Jacko, J.A. Toward a Deeper Understanding of the Role of Interaction in Information Visualization. *IEEE Trans. Vis. Comput. Graph.* **2007**, *13*, 1224–1231. [CrossRef]
30. Buja, A.; Cook, D.; Swayne, D.F. Interactive High-Dimensional Data Visualization. *J. Comput. Graph. Stat.* **1996**, *5*, 78–99. [CrossRef]
31. Ferretti, A.; Passera, E.; Capes, R. End-to-End Implementation and Operation of the European Ground Motion Service (EGMS): Algorithm Theoretical Basis Document. 2021. Available online: https://land.copernicus.eu/user-corner/technical-library/egms-algorithm-theoretical-basis-document (accessed on 10 April 2023).
32. Bredal, M.; Dehls, J.; Larsen, Y.; Marinkovic, P.; Lauknes, T.R.; Stødle, D.; Moldestad, D.A. The Norwegian National Ground Motion Service (InSAR.No): Service Evolution. *AGU Fall Meet. Abstr.* **2019**, *2019*, G13C-0559.
33. Crosetto, M.; Solari, L.; Balasis-Levinsen, J.; Bateson, L.; Casagli, N.; Frei, M.; Oyen, A.; Moldestad, D.A.; Mróz, M. Deformation monitoring at european scale: The copernicus ground motion service. *Int. Arch. Photogramm. Remote Sens. Spat. Inf. Sci.* **2021**, *43*, 141–146. [CrossRef]
34. Crosetto, M.; Solari, L.; Balasis-Levinsen, J.; Casagli, N.; Frei, M.; Oyen, A.; Moldestad, D.A. Ground deformation monitoring at continental scale: The European ground motion service. *Int. Arch. Photogramm. Remote Sens. Spat. Inf. Sci.* **2020**, *43*, 293–298. [CrossRef]
35. Kalia, A.; Frei, M.; Lege, T. BodenBewegungsdienst Deutschland (BBD): Konzept, Umsetzung Und Service-Plattform. *ZfV-Zeitschrift für Geodäsie, Geoinf. und Landmanagement*, 2021. [CrossRef]
36. Hanssen, R.F. Actuele Bodemdalingskaart Nederland. Available online: https://bodemdalingskaart.nl/en-us/ (accessed on 27 March 2024).
37. Rilevamento Elettromagnetico dell'Ambiente (IREA) of Consiglio Nazionale delle Ricerche (CNR) IREA-CNR InSAR WEB GIS. Available online: http://webgis.irea.cnr.it/webgis.html (accessed on 27 March 2024).
38. Soulakellis, N.A.; Novak, I.D.; Zouros, N.; Lowman, P.; Yates, J. Fusing Landsat-5/TM Imagery and Shaded Relief Maps in Tectonic and Geomorphic Mapping. *Photogramm. Eng. Remote Sens.* **2006**, *72*, 693–700. [CrossRef]

39. Kosmas, C.; Gerontidis, S.; Marathianou, M. The Effect of Land Use Change on Soils and Vegetation over Various Lithological Formations on Lesvos (Greece). *Catena* **2000**, *40*, 51–68. [CrossRef]
40. Kosmas, C.; Gerontidis, S.; Detsis, V.; Zafiriou, T.; Marathianou, M. The Island of Lesvos (Greece). In *Medalus Project: Mediterranean Desertification and Land Use. Manual on Key Indicicators of Desertificaton and Mapping Environmentally Sensitive Areas to Desertification*; Kosmas, C., Kirkby, M., Geeson, N., Eds.; European Union: Brussels, Belgium, 1999; Volume 18882.
41. Zouros, N.C. Geomorphosite Assessment and Management in Protected Areas of Greece Case Study of the Lesvos Island–Coastal Geomorphosites. *Geogr. Helv.* **2007**, *62*, 169–180. [CrossRef]
42. Wang, J.; Zouros, N. Educational Activities in Fangshan UNESCO Global Geopark and Lesvos Island UNESCO Global Geopark. *Geoheritage* **2021**, *13*, 51. [CrossRef]
43. Blasco, J.M.D.; Foumelis, M.; Stewart, C.; Hooper, A. Measuring Urban Subsidence in the Rome Metropolitan Area (Italy) with Sentinel-1 SNAP-StaMPS Persistent Scatterer Interferometry. *Remote Sens.* **2019**, *11*, 129. [CrossRef]
44. WorldCover ESA WorldCover. Available online: https://worldcover2020.esa.int/documentation (accessed on 30 August 2023).
45. Hellenic Geological & Mining Research Authority. Available online: https://www.eagme.gr/site/services (accessed on 30 August 2023).
46. OpenStreetMap. Available online: https://www.openstreetmap.org/ (accessed on 30 August 2023).
47. Kalaitzis, P.; Foumelis, M.; Vasilakos, C.; Mouratidis, A.; Soulakellis, N. Interactive Web Mapping Applications for 2D and 3D Geo-Visualization of Persistent Scatterer Interferometry SAR Data. *ISPRS Int. J. Geo-Inf.* **2023**, *12*, 54. [CrossRef]
48. Poncoş, V.; Stanciu, I.; Teleagă, D.; Maţenco, L.; Bozsó, I.; Szakács, A.; Birtas, D.; Toma, Ş.-A.; Stănică, A.; Rădulescu, V. An Integrated Platform for Ground-Motion Mapping, Local to Regional Scale; Examples from SE Europe. *Remote Sens.* **2022**, *14*, 1046. [CrossRef]
49. Laurini, R. *Geographic Knowledge Infrastructure: Applications to Territorial Intelligence and Smart Cities*; Elsevier: Amsterdam, The Netherlands, 2017.
50. Mańk, A.K. Cartographic Symbolization for High-Resolution Displays. Master's Thesis, TU Wien, Vienna, Austria, 2019.
51. Ledermann, F. Minimum Dimensions for Cartographic Symbology—History, Rationale and Relevance in the Digital Age. *Int. J. Cartogr.* **2023**, *9*, 319–341. [CrossRef]